EXPLORING THE EVOLUTION OF LATERAL EARTH PRESSURE USING THE DISTINCT ELEMENT METHOD

M.-C. Weng * **C.-C. Cheng**

Department of Civil and Environmental Engineering
National University of Kaohsiung
Kaohsiung, Taiwan 81148, R.O.C.

J.-S. Chiou

National Center for Research on Earthquake Engineering
Taipei, Taiwan 10668, R.O.C.

ABSTRACT

This study adopted the distinct element method (DEM) to explore the key influencing factors on the variations of lateral earth pressure, including packing type, interior friction angle, particle stiffness and particle size. The reference parameters for the DEM model were retrieved from direct shear tests of a rod assembly. Based on the reference parameters, the evolution of lateral earth pressure is further simulated, and a parametric study was conducted. The results showed that: (1) the analysis model could effectively capture the variation of lateral earth pressure under both active and passive conditions, and the simulated failure patterns were consistent with those from the sandbox tests; (2) the greater interior friction angle $\phi_{interior}$ decreased the active coefficient K_a and increased the passive coefficient K_p; (3) increasing particle stiffness decreased the active coefficient K_a and increased the passive coefficient K_p; (4) larger particle sizes led to a larger active coefficient K_a and a smaller passive coefficient K_p; and (5) when the particle assembly was arranged in order, its lateral pressure was much larger than that of the randomly packed assembly.

Keywords: Distinct element method, PFC2D, Lateral earth pressure.

1. INTRODUCTION

In designing geotechnical structures such as retaining walls and structure foundations, the earth pressure is an important design parameter. Figure 1 shows a typical example of the earth pressure of a wall σ_h' versus the wall displacement ratio of the wall displacement ΔH to the wall height H (Das, [1]). It can be seen that the magnitude of earth pressure depends on the degree of movement of the wall. When the wall is at rest, the earth pressure at this moment is called the at-rest earth pressure. If the wall moves outward, *i.e.*, it has a positive displacement ratio, the earth pressure on the wall decreases, and it will finally reach an active failure state. If the wall moves inward, *i.e.*, it has a negative displacement ratio, the earth pressure on the wall increases, and it will finally reach a passive failure state. Thus, the threshold of the wall displacement ratio in reaching either active or passive failure states depends on the soil type. Conventionally, the soil is idealized as a continuum to estimate the earth pressure. As an extreme case, the soil is further assumed to be rigid and only accounts for the equilibrium of forces, or works on a prescribed failure surface to compute the limit values of earth pressure in the active and passive states, *i.e.* active and passive earth pressures. For example, the well-known Coulomb's theory (Coulomb, [2]) was developed by adopting the limit equilibrium method to search for the most likely plane failure surface that produces an extreme earth pressure value. The active and passive coefficients of earth pressure (K_a and K_p) can be calculated from the following equations, respectively.

$$K_a = \frac{\cos^2(\phi-\theta)}{\cos^2\theta\cos(\delta+\theta)\left[1+\sqrt{\frac{\sin(\delta+\phi)\sin(\phi-\alpha)}{\cos(\delta+\theta)\cos(\theta-\alpha)}}\right]^2} \quad (1)$$

$$K_p = \frac{\cos^2(\phi+\theta)}{\cos^2\theta\cos(\delta-\theta)\left[1-\sqrt{\frac{\sin(\phi-\delta)\sin(\phi+\alpha)}{\cos(\delta-\theta)\cos(\alpha-\theta)}}\right]^2} \quad (2)$$

where ϕ is the friction angle, δ is the soil/wall friction angle, θ is the inclination of the wall to the vertical and α is the inclination of the backfill to the horizontal.

However, many researchers have found experimentally that the theory could not work well in some soils due to its assumption of ideal conditions (Mackey and Kirk, [3]; Naraun *et al.*, [4]; Hung *et al.*, [5]; Fang *et al.*, [6]). In contrast, the finite element method (*FEM*) regards the soil as a deformable elastic-plastic continuum, and can be employed to determine the variation of

* Corresponding author (mcweng@nuk.edu.tw)

DOI : 10.1017/jmech.2013.73
Copyright © 2014 The Society of Theoretical and Applied Mechanics, R.O.C.
https://doi.org/10.1017/jmech.2013.73 Published online by Cambridge University Press

earth pressure in relation to the wall movement as shown in Fig. 1 (Das, [1]; Matsuzawa and Hazarika, [7]). It should be pointed out that soils may not be described as a continuum. Like sands or gravels, they exhibit granular characteristics and have the property of particle separation. The failure pattern of granular materials is often sliding between particles, movements that cannot be interpreted by continuum mechanics. Therefore, it is of key interest to investigate the influence of inter-particle interactions on the development of earth pressure from the viewpoint of particle mechanics.

The distinct element method (DEM), proposed by Cundall (Cundall, [8]; Cundall and Strack, [9]), provides a feasible means to gain more insight into the relationships between the microscopic properties and the macroscopic behavior of granular materials. The DEM has been implemented in the software *PFC2D* and has been widely used to investigate the micro-deformation mechanisms and failure patterns of geo-materials (PFC2D, [10]). The DEM differs from natural geo-material in the following aspects: (1) the shapes of most natural grains are far from circular or spherical and (2) the packing of grains exhibits "linear contact" observed under a microscope, but the contact mode in DEM is mainly "point-to-point" contact between particles. However, many researchers have reported that the behavior of geo-materials can still be adequately captured by DEM despite these simplifications (Calvetti and Emeriault, [11]; Potyondy and Cundall, [12]; Cui and O'Sullivan, [13]; Cho *et al*., [14]; Wang and Leung, [15]; Hsieh *et al*., [16], Schopfer *et al*. [17]). In addition, the DEM has been successfully applied to many areas of engineering, such as soil mechanics, rock engineering, tunneling, and landslide evaluation (Hentz *et al*., [18]; Utili and Nova, [19]; Sitharam *et al*., [20]; Chang and Taboada, [21]).

This study used the DEM implemented in *PFC2D* to investigate the evolution of earth pressure under the plane strain condition, considering the soil as an assembly of particles. Preliminarily, the inter-particle bond and the pore water effect were ignored. Direct shear tests of aluminum-rod assemblies with different packing types were conducted to deduce the reference microscopic properties for the DEM model. Similar tests are also performed to explore the behavior of rod assemblies (Lanier and Jean, [22]; O'Sullivan *et al*., [23]; Ibraim *et al*., [24]). Then, based on the reference properties, a parametric study was performed to explore the influence of microscopic factors, including particle size, particle arrangement, and inter-particle stiffness and friction coefficients, on earth pressure. Additionally, the applicability of the DEM model for lateral earth pressure was validated using sandbox testing of aluminum-rod assemblies.

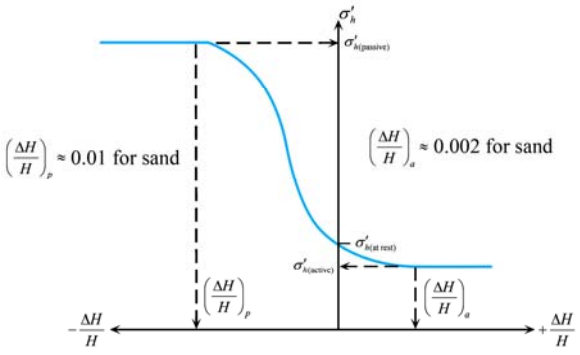


Fig. 1 Variation of lateral earth pressure (Das [1])

2. CONTACT MODEL AND DETERMINATION OF REQUIRED PARAMETERS

2.1 Model Description and Associated Parameters

In *PFC2D*, a basic element represents a rigid circular disk with a finite mass. When one particle contacts with another or a boundary, the particle is allowed to slightly overlap at the contact point and the interaction between particles is described as a soft contact (PFC2D, [10]), which occurs over an infinitely small area. Therefore, a contact force is formed, and it is divisible into normal and shear components with respect to the contact plane. Herein, the linear contact model is adopted, and the normal force of the ith particle F_i^n can be expressed as

$$F_i^n = k^n U^n \tag{3}$$

where U^n is the normal overlap and k^n is the contact normal stiffness.

Similarly, the increment of shear force ΔF_i^s is given by

$$\Delta F_i^s = -k^s \Delta U_i^s \tag{4}$$

where ΔU_i^s is the increment of tangential overlap and k^s is the contact shear stiffness.

Furthermore, the slip between two particles is allowed to occur when the maximum shear force equals the friction, that is $F^s = \mu F^n = tan\ (\phi_{\text{interior}})\ F^n$, where μ is the friction coefficient and ϕ_{interior} is the inter-rod friction angle.

According to the abovementioned contact model, three material parameters, the normal stiffness k^n, the shear stiffness k^s, and the surface friction coefficient between particles μ, are required. These parameters will be determined by simulating the deformation behavior of rod assemblies under a series of direct shear tests.

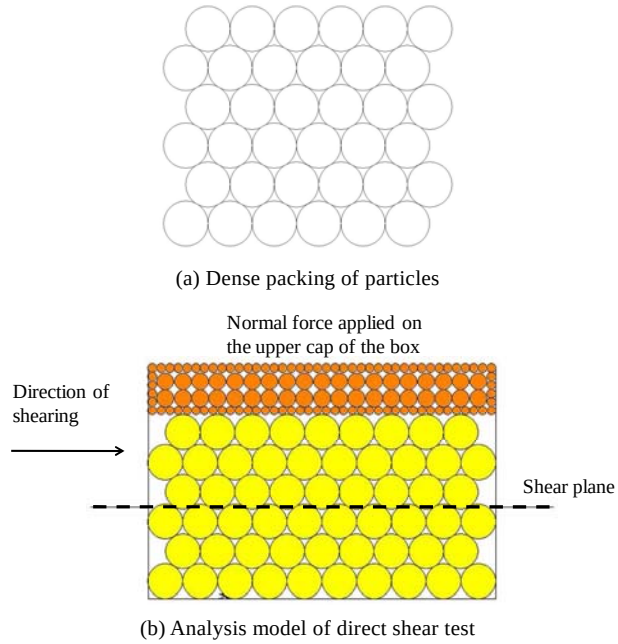
2.2 Direct Shear Test of Aluminum-Rod Assemblies

Considering the uniform geometry and homogeneity of particles, equal-sized circular aluminum rods were selected as the material for the direct shear test. Each rod was 6mm with precision of 0.1mm in diameter and 60mm in length; the material density γ was 2702kg/m^3; the Young's modulus was 70GPa; the Poisson's ratio

https://doi.org/10.1017/jmech.2013.73 Published online by Cambridge University Press

was 0.33. Furthermore, each test specimen had a square cross-section containing six layers of rods, with each layer including 10 rods. Dense packing of particles with a porosity of 9.32% was conducted as shown in Fig. 2. In order to investigate the influence of normal stress, four levels of normal stress were applied: 27.24, 54.48, 108.96 and 217.93kPa. Following this, the specimens under different normal stress levels were sheared at a rate of 1mm/min, based on the ASTM D3080-90 code. For measuring the deformation of each specimen, dial gauges were set up to obtain the horizontal and vertical deformation with a precision of 0.01mm. The shear load was measured by a proving ring attached to the loading frame with an accuracy of 0.294kPa.

Figure 2(b) illustrates a DEM model for simulation of direct shear tests. The specimen of a rod assembly was enclosed by the rigid boundaries. The lateral and lower boundaries were set rigid. The upper boundary was also rigid but allowed to tilt, and it was composed of a series of ball elements with high bond strength and stiffness. During shearing, the lower section of the box was moved forward at a constant velocity the same as the actual test, while the upper section of the box remained stationary. The required parameters were determined by comparing the results of a series of direct shear tests with the simulated results. Through several iterations, a set of microscopic model parameters was determined to ensure that the simulated macroscopic deformational behavior and strength were consistent with the experimental conditions.



(a) Dense packing of particles

(b) Analysis model of direct shear test

Fig. 2 Schematic diagram of dense packing of particles and the analysis model of direct shear test

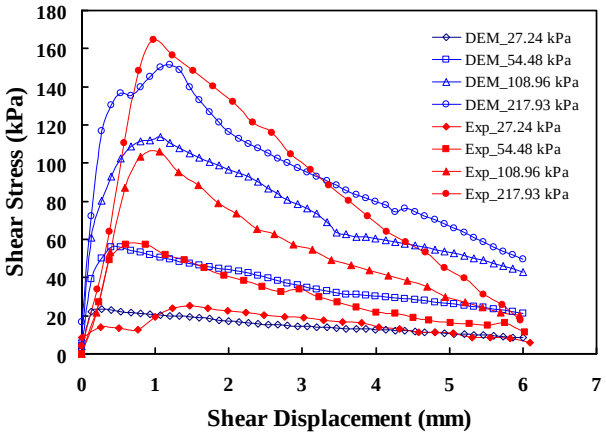
2.3 Verification of Contact Model

Figure 3 shows the stress-displacement curves of the dense packing condition obtained by experiment and numerical simulation. It can be seen the simulated and experimental curves under different normal pressure levels shown in Fig. 3(a) were fairly consistent and the values of peak strength were also similar. Both the simulated and actual behaviors of the aluminum-rod assembly revealed that shear displacements increased linearly at the early shearing stage, and the stiffness increased with increasing application of normal pressure. When the shear stress approached the failure state, strain-softening behavior was observed and stress dropped gradually after the peak. The simulations of volumetric deformation were also similar to the experiment results as shown in Fig. 3(b), and all vertical displacement curves tended to be dilative during the whole shearing process. Accordingly, the set of parameters shown in Table 1 was determined as the reference parameters to be used for the subsequent parametric analysis.

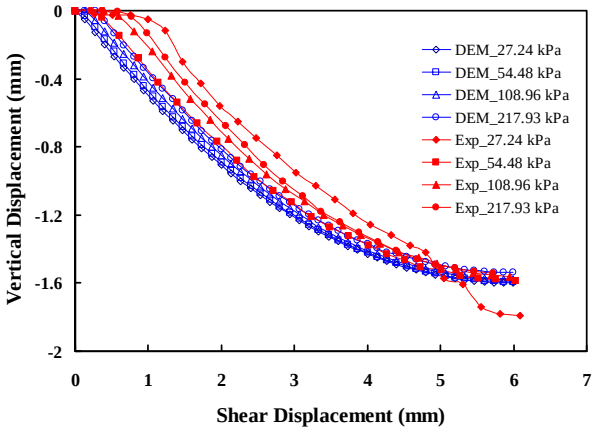
The strength of the rod assembly was also determined using the Mohr-Coulomb expression as follows

$$\tau_f = \sigma \tan\phi + c \tag{5}$$

where τ_f and σ are the shear strength and normal stress respectively, and the parameters ϕ and c are the macroscopic friction angle and the cohesive intercept of the failure envelope, respectively.



(a) Shear stress versus shear displacement



(b) Vertical displacement versus shear displacement

Fig. 3 Comparison of simulated and actual deformations of the rod assembly with dense packing subjected to shearing under various hydrostatic stresses

https://doi.org/10.1017/jmech.2013.73 Published online by Cambridge University Press

Table 1 Microscopic properties of particles for DEM analysis

Property	Value (units)
Density	2702kg/m^3
Normal stiffness k^n	10.35MN/m
Shear stiffness k^s	1.95MN/m
Inter-rod friction angle $\phi_{interior}$	20.9°

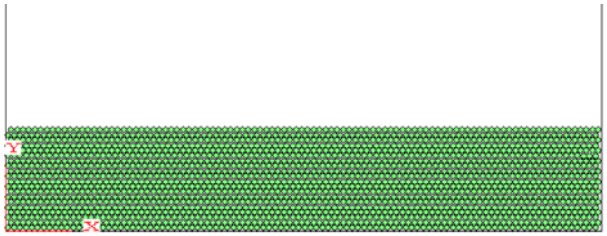
For dense packing, the failure envelope is nearly linear with no cohesion and can be expressed as:

$$\tau_f = \sigma \tan 45.9° \quad (6)$$

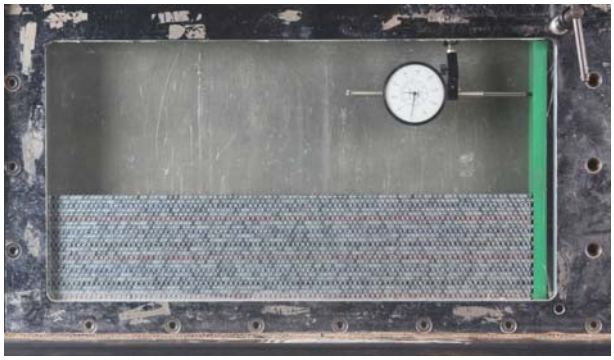
With the above strength parameters, the coefficients of earth pressure for active and passive states based on the conventional plastic theory were evaluated, as presented in the following section.

3. DEM MODEL AND SANDBOX TEST FOR LATERAL EARTH PRESSURE STUDY

Based on the contact model and parameters described above, this study further explored the influences of different packing and microscopic properties of cohesion-less particles on the variations of lateral earth pressure. For dense packing, for example, a numerical model containing 20 layers of rods, each has 100 rods was constructed, as shown in Fig. 4(a). The left side and the bottom of the model were considered as rigid boundaries, and the top of the model was set as an unconstrained boundary. For the right side of the model, a moveable boundary was adopted to simulate the wall sliding along the base. As the wall moved to the right, the earth pressure would develop an active state; as the right wall moved to the left, the earth pressure would develop a passive state. In this simulation, the wall was moved at a constant velocity of 0.1mm/s. For considering the influence of particle packing, two types of packing, dense packing and random packing, of which the porosities were about 20.7%, were investigated. The term "random packing" herein means that the particles uniformly drop into the container from a fixed height and the particle assemblies pack by gravity without any compaction and arrangement. Based on these packing types, numerical analyses with different inter-particle friction angles, stiffness values, and rod sizes were conducted to systematically study the corresponding variations in earth pressure. The interior friction angle was chosen from the range ($\phi_{interior}$) to ($\phi_{interior} + 20°$), in which the corresponding friction coefficient ranged from 0.284 to 0.865. The normal stiffness ranged from 0.1 k^n to 100 k^n, of which the magnitude was between 1.035MN/m to 1035MN/m, considering the variety of deformation modulus of geo-material (Das, [1]). The assigned shear stiffness k^s also increase in proportion to the increase of normal stiffness. To explore the size effect, four rod diameters were chosen as 1.5mm, 3mm, 6mm and 12mm.



(a) DEM simulation



(b) Sandbox test

Fig. 4 Schematic illustration of lateral earth pressure test

Before the parametric study described above was conducted, sandbox tests with an aluminum-rod assembly for lateral earth pressure were performed for further checking the appropriateness of the numerical model and the set parameters. As shown in Fig. 4(b), the size of the aluminum-rod assembly was 600mm in width by 300mm in height, and a lateral frictionless steel wall (42mm wide) was set at the right side of the rods and the wall is driven by an oil jack, which exerts force at the 1/3 height of the rod assembly. A load cell is attached between the wall and the oil jack to measure actual force. Then, the earth pressure coefficient K_h could be obtained from $K_h = 2P/\gamma H^2$, where P is the force measured from the load cell and H is the height of the rod assembly. Hence, the failure patterns and the variation of earth pressure for different types of packing could be compared with those from the DEM analyses.

4. SIMULATIONS AND RESULTS

4.1 Failure Pattern

When the wall was moved outward, *i.e.* in an active condition, the rods near the wall would collapse because of the loss of support from the wall. Figure 5 illustrates a series of experimental pictures under this condition. The initial active failure plane can be observed in Fig. 5(b) at the wall movement of 2.64mm. Furthermore, Fig. 6 compares the failure patterns of the experiments with the DEM analyses for the two types of particle packing, respectively. It can be seen that the patterns from the analyses are similar to those from the experiments, which is also close to the theoretical failure plane of (45°−ϕ/2) in dense packing condition (Fig. 6(a)). When the wall was moved inward, *i.e.* in a passive condition, the surface of the rod assembly near

https://doi.org/10.1017/jmech.2013.73 Published online by Cambridge University Press

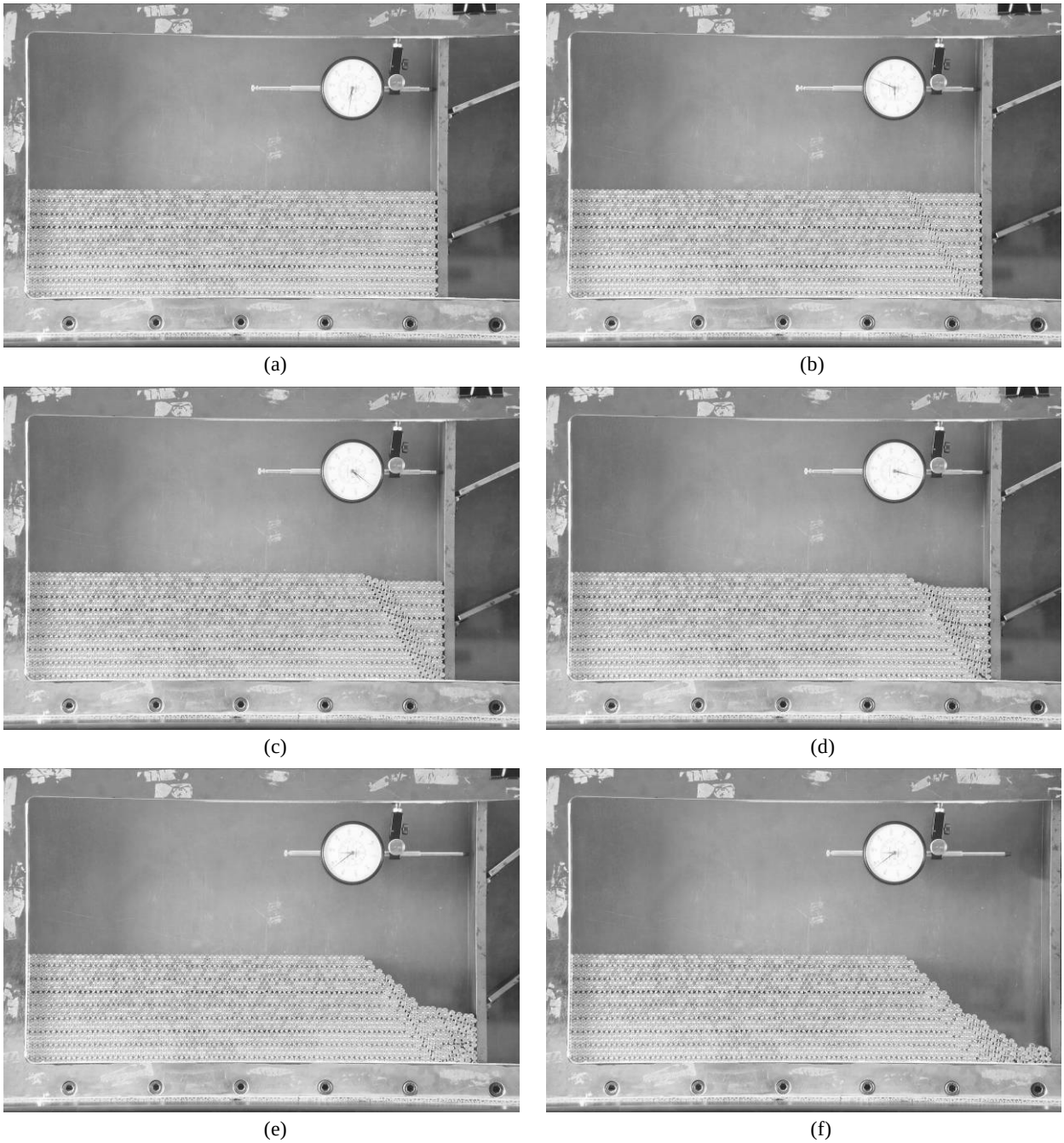


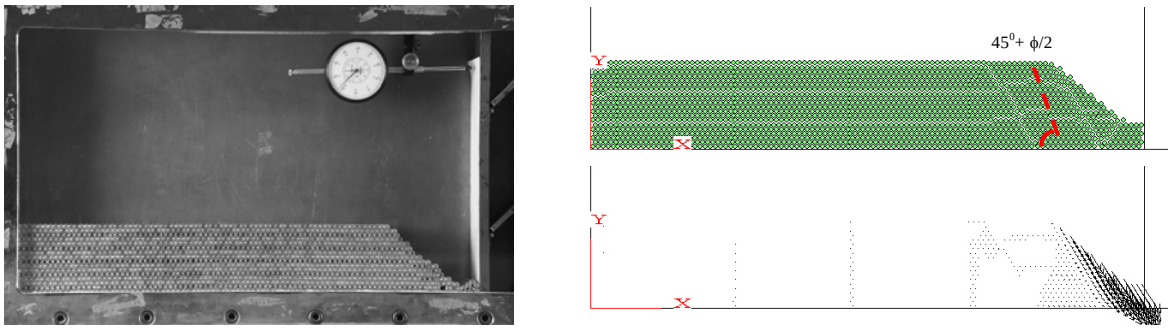
Fig. 5 Sliding process of the rod assembly under active earth pressure condition

the wall would heave due to the compression of the wall. For this condition, Fig. 7 shows consistent failure patterns between the experiments and numerical analyses for the two packing types. However, these failure planes are much steeper than the theoretical failure plane of $(45° + \phi/2)$ (Fig. 7(a)).

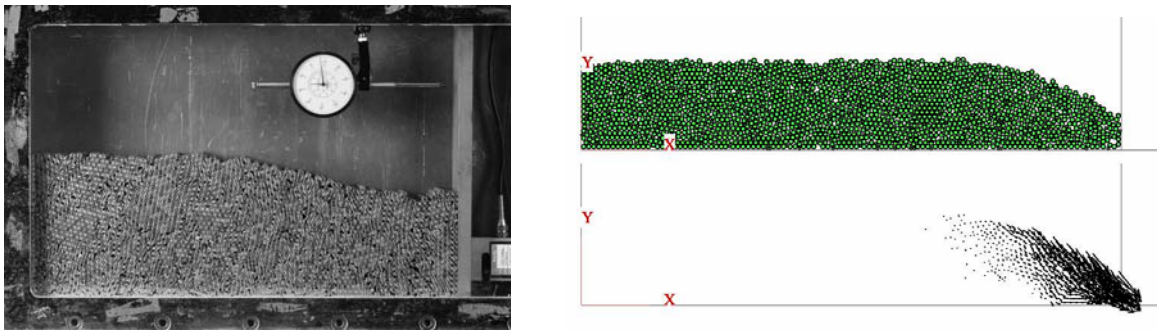
4.2 Variations of Lateral Earth Pressure

Figure 8 further compares the variations of the coefficients of lateral earth pressure deduced from the experiments with those from the analyses for the inward wall movement. Their trends were found to be similar. For dense packing, the coefficient of earth pressure initially increased with increasing wall movement and reached a peak at about 1% of the displacement ratio. The peak values from DEM analysis and experimental were 72.4 and 85.3, respectively. These values are much higher than those commonly used in engineering practice. After the peak, the coefficient of earth pressure gradually decreased with increasing movement, reflecting the dilation mode of dense sand. For the random packing condition, the coefficient of earth pressure increased with increasing wall movement. At about 1% of displacement ratio, the coefficient of earth pressure reached the ultimate value and exhibited a fairly ductile behavior, similar to that of loose sand.

https://doi.org/10.1017/jmech.2013.73 Published online by Cambridge University Press

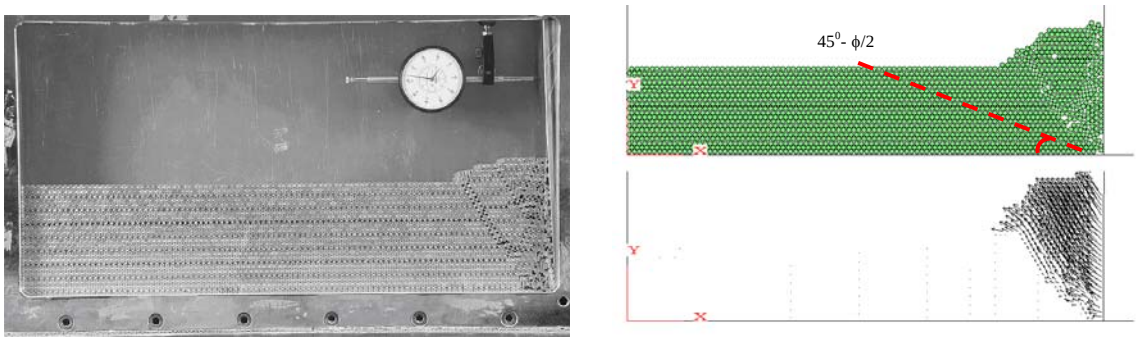


(a) Dense packing

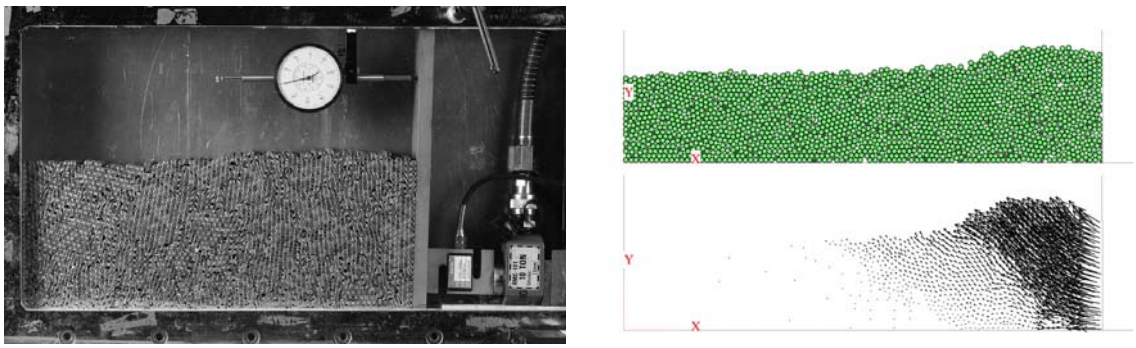


(b) Random packing

Fig. 6 Failure patterns of the rod assembly under active earth pressure condition



(a) Dense packing



(b) Random packing

Fig. 7 Failure patterns of the rod assembly under passive earth pressure condition

https://doi.org/10.1017/jmech.2013.73 Published online by Cambridge University Press

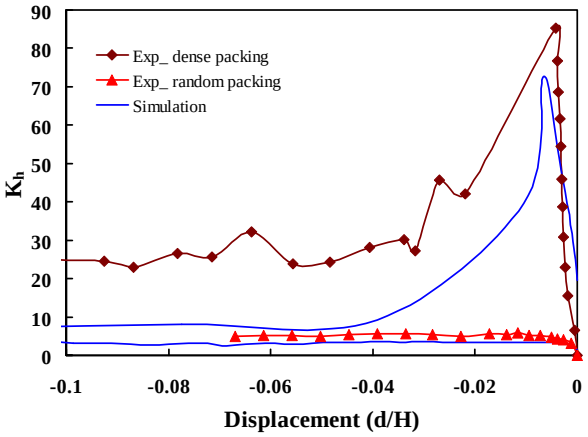


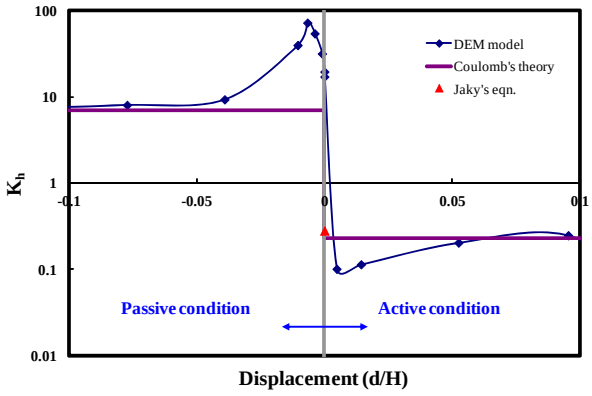
Fig. 8 Comparison of simulated and actual coefficients of lateral earth pressure under passive condition

Another comparison between the coefficient of earth pressure from analysis and conventional plastic theory was performed (Fig. 9). With the above strength parameters of Mohr-Coulomb criteria, the coefficients of active and passive earth pressure were calculated based on Coulomb's theory. In addition, the coefficient of earth pressure at rest based on Jaky's solution ($K_0 = 1 - \sin\phi$) is also plotted in Fig. 9. For dense packing, Fig. 9(a) compares the variation of the earth pressure coefficient K_h from the DEM analysis with Coulomb's theory using $\phi = 45.9°$ and $\delta = 45.9°$ (Eq. 1). It can be seen that under the active condition, the values of K_h at large displacement were close to those from the Coulomb's theory. However, under the passive condition, a significant difference was found between the DEM analysis and Coulomb's theory. The peak value of the DEM analysis was much greater than that based on Coulomb's theory, with value is 6.91. In addition, as the displacement increases, the ultimate value of the DEM analysis approaches that of Coulomb's theory. For random packing as shown in Fig. 9(b), it can be seen that for the passive state, the value of K_h at large displacement agreed well with that from Coulomb's theory, while for the active state, the value of K_h at large displacement was a little higher than that from Coulomb's theory. The overall agreement was fairly good. From the above comparisons, Coulomb's theory seems to be more suitable for the random packing of particles. As the particles became arranged in order, Coulomb's theory would underestimate the passive earth pressure.

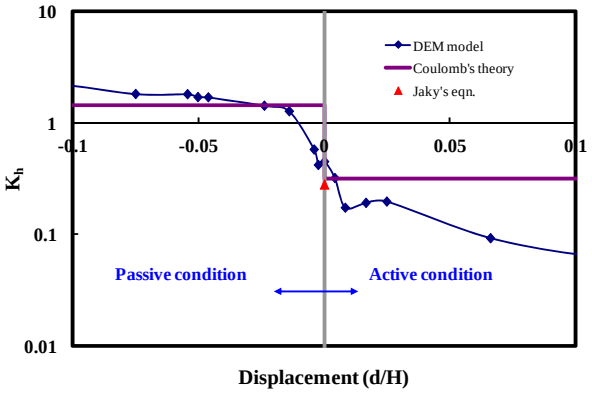
Based on the simulation of lateral earth pressure, this study was able to further validate the adopted DEM model and use the associated model parameters as reference values in the parametric study described in the following section.

5. INFLUENCING FACTORS ON THE COEFFICIENTS OF EARTH PRESSURE

The influence of microscopic factors, including particle arrangement, interior friction angle, stiffness, and



(a) Dense packing



(b) Random packing

Fig. 9 Variations of coefficient of lateral earth pressure under different packing conditions

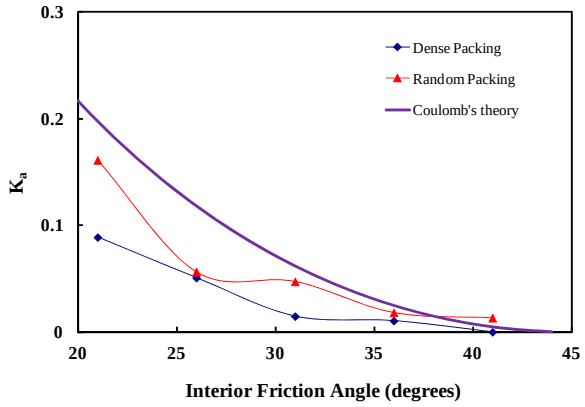
particle size on the active and passive earth pressure coefficients are investigated in this section. As suggested by Das [1], and shown in Fig. 1, active earth pressure occurs when the lateral displacement reaches a magnitude of 0.002 of the height of the retaining wall (0.002 H); the earth pressure reaches the passive state when the lateral displacement equals 0.01 H. Therefore, the active and passive earth pressure coefficients, K_a and K_p, can be accordingly determined from the simulated stress-displacement curves.

5.1 Influence of Interior Friction Angle

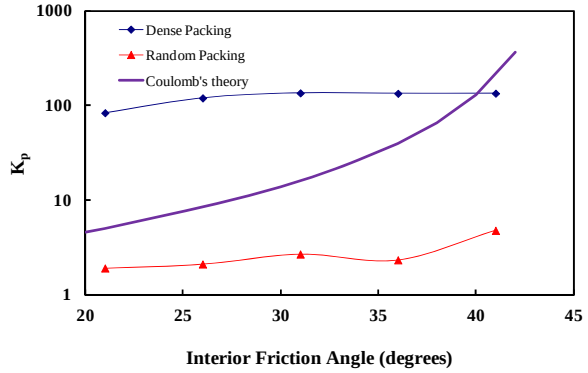
Figure 10 depicts the variations of the earth pressure coefficients with different interior friction angles of particles, ranging from 20.8° to 40.8°. The theoretical results of Coulomb's theory are also plotted for comparison. For the active condition as shown in Fig. 10(a), it could be seen that increasing interior friction angle $\phi_{interior}$ decreased the active coefficient K_a in all packing types. These tendencies agree with that of Coulomb's theory, especially for the variation of random packing, which is much more similar to that of Coulomb's theory.

On the other hand, an increase in $\phi_{interior}$ led to an increase in the passive coefficient K_p as shown in Fig. 10(b). Although the tendencies of variation were similar, the magnitudes of dense packing were much greater than that of random packing. For this packing type,

https://doi.org/10.1017/jmech.2013.73 Published online by Cambridge University Press



(a) Active condition



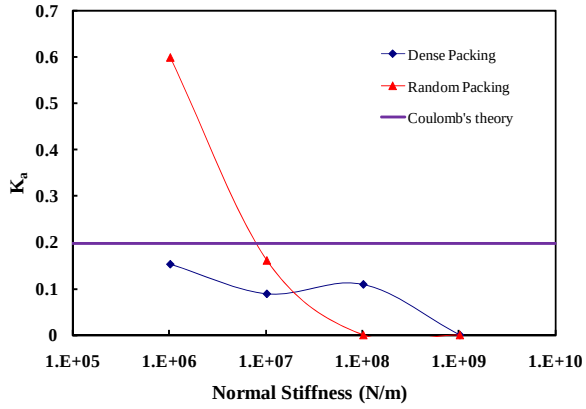
(b) Passive condition

Fig. 10 Variation of the coefficient of lateral earth pressure with different friction angles

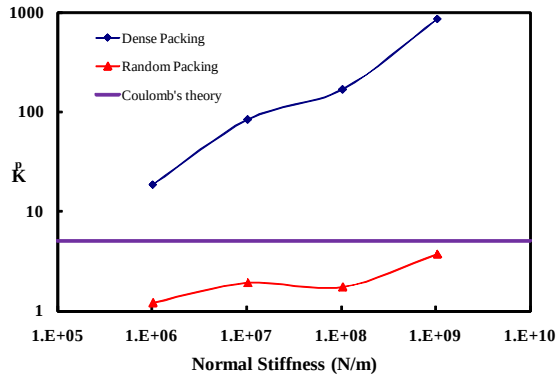
owing to the particles arrangement in order, the contact forces between particles could completely develop and the exhibited resistant force became much larger. Furthermore, it was found that Coulomb's passive pressure exhibited a very wide range of variation. The Coulomb pressure was similar to that of random packing at a low friction angle (about 20°), and it increased rapidly and approached the values of dense packing at a high angle (after 38°). These results indicate that the tendencies of the two analysis methods are similar, but the coefficient values of earth pressure are apparently different.

5.2 Influence of Stiffness

Figure 11 illustrates the variations of the earth pressure coefficients with different particle stiffness. The theoretical results of Coulomb's theory ($\phi_{interior} = 20.8°$) are also plotted for comparison. For the active condition as shown in Fig. 11(a), increasing particle stiffness decreased the active coefficient K_a in all packing types. Furthermore, an increase in the stiffness led to an increase in the passive coefficient K_p as shown in Fig. 11(b). Conventionally, the earth pressure evaluation of limit equilibrium theory depends only on the friction angle, the cohesion, and the density of geo-material and it does not consider the deformation of geo-material. However, in this study, it was found that the magnitude of earth pressure is significantly affected by the stiffness, as shown in Fig. 11. As compared to the influence of the friction angle, the particle stiffness seems more significant.



(a) Active condition



(b) Passive condition

Fig. 11 Variation of the coefficient of lateral earth pressure with different particle stiffness

5.3 Influence of Particle Size

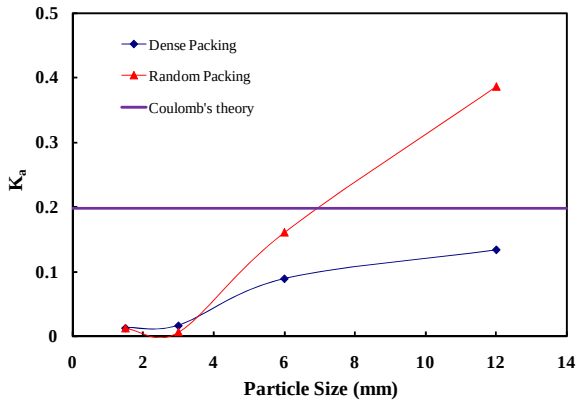
Figure 12 illustrates the simulated earth pressure coefficient versus different particle sizes. Figure 12(a) shows how the active coefficient K_a of dense packing increased as the particle size increased. Especially for the random packing, the coefficient K_a is significantly influenced by the particle size. For the passive condition as shown in Fig. 12(b), the larger size induced the lower passive coefficient K_p.

6. CONCLUSIONS

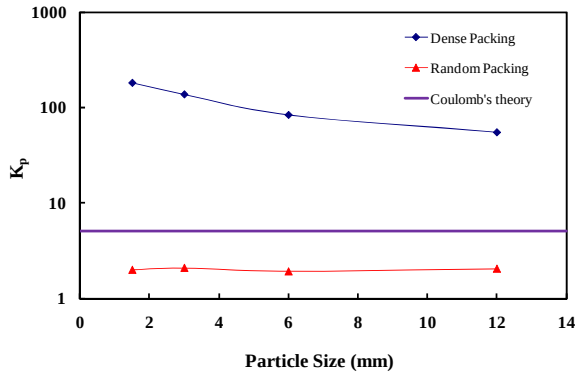
This study explored the influencing factors, including the packing type, the interior friction angle, the particle stiffness and the particle size, on the variations of lateral earth pressure. The software PFC2D based on the distinct element method (DEM) was adopted. The DEM model was tested for modeling direct shear tests and showed good capability in simulating and predicting the macroscopic mechanical behavior of a rod assembly under different stress states. On such a basis, the lateral earth pressure evolution was further simulated by the DEM model and the simulation results showed the following:

1. The analysis model could effectively capture the variations of lateral earth pressure under both active and passive conditions, and the simulated failure patterns were consistent with those from the sandbox tests.

https://doi.org/10.1017/jmech.2013.73 Published online by Cambridge University Press



(a) Active condition



(b) Passive condition

Fig. 12 Variation of coefficient of lateral earth pressure with different particle sizes

2. The greater interior friction angle $\phi_{interior}$ led to the lower active coefficient K_a and increased the passive coefficient K_p. These tendencies agreed with that of the conventional limit equilibrium theory, but the values of the two analysis methods exhibited significant differences.
3. Increasing inter-particle stiffness decreased the active coefficient K_a and increased the passive coefficient K_p. The larger particle size led to the higher active coefficient K_a and the lower passive coefficient K_p
4. When the assembly was arranged in order, such as dense packing, it exhibited much larger lateral pressure than for the random packing.

The packing type, particle stiffness and particle size are not considered in the conventional limit equilibrium theory. The DEM analysis in this study has shown that these factors indeed affect the evolution of lateral earth pressure.

REFERENCES

1. Das, B. M., *Principles of Geotechnical Engineering*, Brooks/Cole Publishing Company (2010).
2. Coulomb, C. A., "Essai Sur Une Application Des Regles De Maximis a Quelques Problems De Statique," *Relatifs a l'Architecture. Mémoires de Marhématique de l'Académie Royale des Sciences, Paris*, p. 3 (1776).
3. Mackey, R. D. and Kirk, D. P., "At Rest, Active and Passive Earth Pressure," *Proc. South East Asian Conf. on Soil Mechanics and Foundations Engineering*, Bangkok, pp. 187–199 (1967).
4. Naraun, J., Saran, S., Nandakumaran, P., "Model Study of Passive Pressure in Sand," *Journal of Soil Mechanics and Foundations Engineering*, ASCE, **95**, pp. 969–983 (1969).
5. Hung, C. C., Menq, F. Y. and Chou, Y. C., "The Effect of the Bending Rigidity of a Wall on Lateral Pressure Distribution," *Canadian Geotechnical Journal*, **36**, pp. 1039–1055 (1999).
6. Fang, Y. S., Ho, Y. C., Chen, T. J., "Passive Earth Pressure with Critical State Concept," *Journal of Geotechnical and Geoenvironmental Engineering*, **128**, pp. 651–659 (2002).
7. Matsuzawa, H. and Hazarika, H., "Analyses of Active Earth Pressure Against Rigid Retaining Wall Subjected to Different Modes of Movement," *Soils and Foundations*, **36**, pp. 51–65 (1996).
8. Cundall, P. A., "A Computer Model for Simulating Progressive, Large Scale Movement in Blocky Rock Systems," *Proceedings of the symposium of international society of rock mechanics*, Nancy, France, **2**, pp. 129–136 (1971).
9. Cundall, P. A. and Strack, O. D. L., "A Discrete Numerical Model for Granular Assemblies," *Geotechnique*, **29**, pp. 47–65 (1979).
10. PFC2D (Particle Flow Code in 2 Dimension). Version 4.0., Minneapolis: Itasca Cons Group (2004).
11. Calvetti, F. and Emeriault, F., "Interparticle Forces Distribution in Granular Materials: Link with the Macroscopic Behaviour," *Mechanics of Cohesive-Frictional Materials*, **4**, pp. 247–279 (1999).
12. Potyondy, D. O. and Cundall, P. A., "A Bonded-Particle Model for Rock," *International Journal of Rock Mechanics and Mining Science*, **41**, pp. 1329–1364 (2004).
13. Cui, L. and O'Sullivan, C., "Exploring the Macro- and Micro-Scale Response of an Idealised Granular Material in the Direct Shear Apparatus," *Geotechnique*, **56**, pp. 455–468 (2006).
14. Cho, N., Martin, C. D. and Sego, D. C., "A Clumped Particle Model for Rock," *International Journal of Rock Mechanics and Mining Science*, **44**, pp. 997–1010 (2007).
15. Wang, Y. H. and Leung, S. C., "A Particulate-Scale Investigation of Cemented Sand Behaviour," *Canadian Geotechnical Journal*, **45**, pp. 29–44 (2008).
16. Hsieh, Y. M., Li, H. H., Huang, T. H. and Jeng, F. S., "Interpretations on How the Macroscopic Mechanical Behavior of Sandstone Affected by Microscopic Properties—Revealed by Bonded-Particle Model," *Engineering Geology*, **99**, pp. 1–10 (2008).
17. Schopfer, M. P. J., Abe, S., Childs, C. and Walsh, J. J., "The Impact of Porosity and Crack Density on the

https://doi.org/10.1017/jmech.2013.73 Published online by Cambridge University Press

Elasticity, Strength and Friction of Cohesive Granular Materials: Insights from DEM Modeling," *International Journal of Rock Mechanics and Mining Science*, **46**, pp. 250–261 (2009).

18. Hentz, S., Daudeville, L. and Donze, F., "Identification and Validation of a Discrete Element Model for Concrete," *Journal of Engineering and Mechanics*, **130**, pp. 709–719 (2004).
19. Utili, S. and Nova, R., "DEM Analysis of Bonded Granular Geomaterials," *International Journal for Numerical and Analytical Methods in Geomechanics*, **32**, pp. 1997–2031 (2008).
20. Sitharam, T. G., Vinod, J. S. and Ravishankar, B. V., "Evaluation of Undrained Response from Drained Triaxial Shear Tests: DEM Simulations and Experiments," *Geotechnique*, **58**, pp. 605–608 (2008).
21. Chang, K. J. and Taboada, A., "Discrete Element Simulation of the Jiufengershan Rock-And-Soil Avalanche Triggered by the 1999 Chi-Chi Earthquake, Taiwan," *Journal of Geophysical Research*, **114**, F03003, doi: 10.1029/2008JF001075 (2009).
22. Lanier, J. and Jean, M., "Experiments and Numerical Simulations with 2D Disks Assembly," *Powder Technology*, **109**, pp. 206–221 (2000).
23. O'Sullivan, C., Bray, J. D. and Riemer, M. F., "Influence of Particle Shape and Surface Friction Variability on Response of Rod-Shaped Particulate Media," *Journal of Engineering Mechanics*, **128**, pp. 1182–1192 (2002).
24. Ibraim, E., Lanier, J., Wood, M. D. and Viggiani, G., "Strain Path Controlled Shear Tests on an Analogue Granular Material," *Geotechnique*, **60**, pp. 545–559 (2010).

(Manuscript received July 6, 2011,
accepted for publication September 21, 2012.)

https://doi.org/10.1017/jmech.2013.73 Published online by Cambridge University Press